J Therm Anal Calorim (2011) 104:299–306
DOI 10.1007/s10973-010-1171-4

Spectroscopic and structural study of the ambazone hydrochloride

Marieta Muresan-Pop · Irina Kacsó · Carmen Tripon · Z. Moldovan · Gh. Borodi · S. Simon · I. Bratu

Received: 2 August 2010 / Accepted: 8 November 2010 / Published online: 14 December 2010

Abstract Ambazone, a well-known antimicrobial compound, presents also oncostatic properties. The solid form, obtained by using solvent-drop grinding procedure, was characterized by using several physical techniques such as FTIR, X-ray photoelectron spectroscopy, ^{13}C NMR and ^{15}N NMR spectroscopies, thermal analysis, X-ray powder diffraction and mass spectrometry. Based on these data, it was demonstrated that an ambazone–hydrochloride was obtained: new vibrations corresponding to NH_2^+ were identified. DTA–TG–DSC and MS data revealed that a new crystal type has been obtained. X-ray diffraction data allowed the determination of the lattice parameters and the most probable space group $P_{21/c}$ was established also with only one molecule per asymmetric unit.

Keywords Ambazone · Antiseptic · Guanidines · X-ray powder diffraction · DTA–TG–DSC · FTIR · ^{13}C NMR · XPS · Spectroscopy

Introduction

Ambazone monohydrate, $C_8H_{11}N_7S{\cdot}H_2O$ ([4-(2-(Diaminomethylidene)hydrazinyl)phenyl] iminothiourea), (AMB, Fig. 1) one of the oldest antimicrobial chemicals is a dark-brown, odorless, tasteless microcrystalline powder having the melting point around at 192 up to 194 °C with decomposition. With a very slightly solubility in water and in the other organic solvents, it presents a bacteriostatic action on hemolytic streptococcus, streptococcus pneumonias, and viridians' streptococcus, being employed as local bacteriostatic in the buccal cavity. The studies performed during the 1950–1960 period have shown the local antibacterial properties when it is administrated at the buccal pharyngeal cavity level, being an efficient antimicrobial drug [1]. The ulterior re-evaluation of the antibacterial AMB properties evidenced an antibacterial activity spectrum similar to that of sulfamides [2]. Recently, the antineoplasm properties of AMB were also demonstrated [3–9], that accelerated the researches on this substance, without mutagenic effects [10] and unpleasant reactions characteristic to other oncostatic drugs [2] (Fig. 1).

Traditionally, the solid form selection process was limited to the free drug or pharmaceutically accepted salts [11]. Based on this choice, the form with the best properties for the intended usage was developed. Polymorphs, co-crystals, solvates or salts, exhibit different properties compared with free drugs and can now significantly increase the options for the development of different solid forms. Salts differ from other solid forms in the following way: in salts, a proton is transferred from the acidic to the basic functionality of the crystallization partner, as the *pKa* difference between the partners is sufficiently large [12].

The solid form influences relevant physical-chemical parameters such as solubility, dissolution rate of the drug, chemical stability, melting point, and hygroscopic parameter which can result in solids with superior properties.

If the bioavailability is strongly influenced by the solubility and the dissolution profile, these can have significant consequences and determine if the compound is further developed.

M. Muresan-Pop · S. Simon
Faculty of Physics, Babes-Bolyai University, Cluj-Napoca, Romania

I. Kacsó · C. Tripon · Z. Moldovan · Gh. Borodi · I. Bratu (✉)
National Institute for R&D of Isotopic and Molecular Technologies, P.O. Box 700, 400293 Cluj-Napoca, Romania
e-mail: ibratu@itim-cj.ro

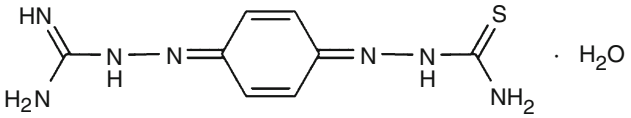

Fig. 1 Ambazone monohydrate molecule

In recent years, much of the research has been carried out on the preparation of pharmaceutical solid forms. Usually, there are two methods by which solid forms may be prepared: solution-based crystallization and grinding. Mechanical chemical methods [13–18], more commonly and usefully described as grinding, have been employed extensively in the preparation of solid forms. The range of grinding conditions has been extended by the addition of solvents in the "*solvent-drop*" method [18] and this may represent the introduction of solution conditions on a limited scale to the grinding process. The obtained solid form was characterized by several physical methods such as X-ray powder diffraction, FTIR, ^{13}C NMR, ^{15}N NMR, X-ray photoelectron spectroscopy (XPS), thermal analysis, and mass spectrometry. The chosen methods demonstrate the formation of the ambazone hydrochloride compound.

Experimental

Solvent-drop grinding procedure

More recently, the use of so-called "*solvent-drop*" grinding has been developed, in which a small quantity of a solvent is added to the solid substance or mixture prior to grinding [19].

The Ambazone was obtained from *Microsin* SRL Bucharest, Romania, and was used without further purification. The Ambazone hydrochloride (AMB·HCl) was prepared by grinding of 255.3 mg AMB with 2 mL HCl aqueous solution (0.5 M) in an agate mortar at room temperature, until a dried compound was obtained.

X-ray powder diffraction

X-ray powder diffraction pattern was obtained using Bruker D8 Advance diffractometer, sealed Cu tube $\lambda = 1.5406$ Å equipped with an incident beam Ge 111 monochromator.

FTIR spectroscopy

FTIR spectra were obtained with a JASCO 6100 FTIR spectrometer in the 4000 to 400 cm^{-1} spectral domain with a resolution of 4 cm^{-1} using KB pellet technique.

Thermal analysis DSC–DTA–TG

Differential scanning calorimetry (DSC) was carried out by means of a Shimadzu DSC-60 calorimeter, the sample was heated in the range of 30–350 °C with a heating rate of 10 °C/min in crimped aluminum sample cell. The purge gas was a nitrogen flow of 60 mL/min. For data collection the Shimadzu TA-WS60 and TA60 2.1 softwares were employed.

Differential thermal analysis (DTA) and thermogravimetry (TG) were obtained with a Simultaneous Thermogravimetric and Differential Thermal Analyzer from Shimadzu type *DTG-60/60H*. The measurements were performed by using alumina cells (Ø5.8 mm × 2.5 mm). The sample was heated in the range 30–350 °C with a heating rate of 10 °C/min in alumina sample cell under dry nitrogen purge (70 mL/min).

Mass spectrometer

Mass spectrometer Finnigan Mat 311 with electron impact settee at 70 eV was used. The mass range was 25–400 Daltons. The introduction system was heated in the range 25–350 °C with a heating rate of 25 °C/min. The mass spectra were collected in continuous mode at a velocity of one mass spectrum at every 5 s.

^{13}C NMR spectroscopy

Solid-state cross-polarization magic-angle-spinning (CP/MAS) NMR spectra were recorded at 600 MHz ^{1}H Larmor frequency with a Bruker AVANCE III spectrometer. The SS-NMR experiment was performed on AMB and AMB·HCl compounds at room temperature. The samples were center-packed to minimize the effect of *rf* field inhomogeneity. Standard CP/MAS experiments were performed at a spinning frequency of 10 kHz for ^{13}C and 7 kHz for ^{15}N, using a ^{1}H 90° pulse length of 3 and 4.2 μs, respectively. The CP/MAS NMR spectra were acquired under two-pulse phase-modulated ^{1}H decoupling at 100 kHz by averaging 20,000 scans for ^{13}C, and 130,000 scans for ^{15}N, with a recycle delay of 3 s. The CP transfer was optimized for the first Hartmann–Hahn matching condition, where the *rf* fields on the ^{1}H channel has been calibrated to 60 kHz. The contact pulse was set to 1.5 ms in the ^{13}C case, and to 5 ms for ^{15}N. The ^{13}C CP/MAS spectra of the AMB and AMB·HCl are calibrated according to the $^{13}CH_3$ line in TMS through an indirect procedure which uses as an intermediary standard the ^{13}C SS-NMR resonance lines of glycine. Chemical shifts for ^{15}N were calibrated indirectly on glycine resonance ($^{15}NH_3^+$ at 0 ppm), and referenced to CH_3NO_2 signal.

X-ray photoelectron spectroscopy

XPS measurements were performed using a SPECS PHOIBOS 150 MCD system equipped with monochromatic AlKα source (250 W, $h\nu = 1486.6$ eV), hemispherical analyzer, and multichannel detector. The typical vacuum in the analysis chamber during the measurements was in the range of 10^{-9}–10^{-10} mBar. Charge neutralization was used for all samples. The binding energy scale was charge referenced to the C 1s at 284.6 eV. Elemental compositions were determined from spectra acquired at the pass energy of 100 eV. High-resolution spectra were obtained using analyzer pass energy of 30 eV and Shirley background subtraction method was used for fitting procedure.

Results and discussion

X-ray powder diffraction

X-ray powder diffraction pattern for AMB and diffraction pattern for AMB·HCl are presented in Fig. 2. One can see that these two diffraction patterns are totally different and a solid form of AMB was obtained.

From powder pattern indexing by using Dicvol method [20] it was established that AMB·HCl crystallized in monoclinic system having following lattice parameters: $a = 7.006$ Å, $b = 13.017$ Å, $c = 16.959$ Å, and $\beta = 107.17°$. The unit cell volume is $V = 1477$ Å^3. The most probable space group obtained from reflections systematic absences is $P_{21/c}$. The calculated density, if we consider four molecules in the unit cell which is characteristic for this space group, is 1.23 g/cm^3. This is a reasonable value for such a compound.

In order to characterize the crystallinity of the new compound the crystallite size was evaluated using Scherer formula and we have obtained the following sizes: 1176 Å for AMB·HCl comparative to AMB which has 1361 Å. No impurity's diffraction lines were detected by X-ray diffraction.

FTIR spectroscopy

The band at $\sim$3400 cm^{-1} can be assigned to N–H stretching from primary amine in pure ambazone (see Fig. 3). The band at 3425 cm^{-1} can be assigned to O–H [21], or N–H stretching of water or amine in AMB·HCl; it can be observed also as a shoulder in the spectrum of AMB·HCl.

In the case of AMB, the FTIR spectrum contains two NH_2 vibrations (3300 and 3500 cm^{-1}) [22, 23] and NH (3320–3180 cm^{-1}, i.e., 3226 cm^{-1}) for pure ambazone [23, 24].

Salt formation has been shown to modify the NH-stretching absorption in amines [23, 25]; it was observed that the free bases have a sharp strong band at $\sim$3226 cm^{-1} due to the NH stretching and that this band is greatly reduced in intensity in the spectra of the hydrochlorides. The band at 3146 cm^{-1} corresponds to the NH vibration [23] for pure AMB. The band at 3134 cm^{-1} can be assigned to N–H stretching of secondary amine in salt spectrum. New bands appear between 3200 and 2000 cm^{-1}, i.e., at $\sim$2980 cm^{-1} probably due to the protonated secondary amine [23].

Primary amine has an absorption band of medium intensity at $\sim$1613 cm^{-1} (see Fig. 4), being located at $\sim$1612 cm^{-1} by salt formation [25]. Cleaves and Phyler [26] correlated the spectral bands at 1625–1516 cm^{-1} with NH deformation vibration. The pure ambazone spectrum

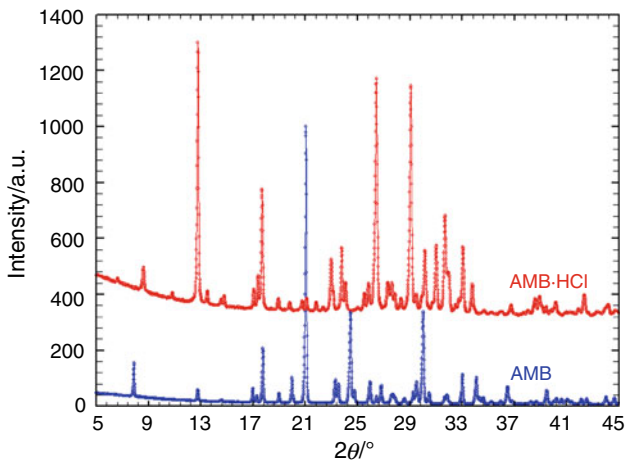

Fig. 2 X-ray powder diffraction pattern for AMB and AMB·HCl

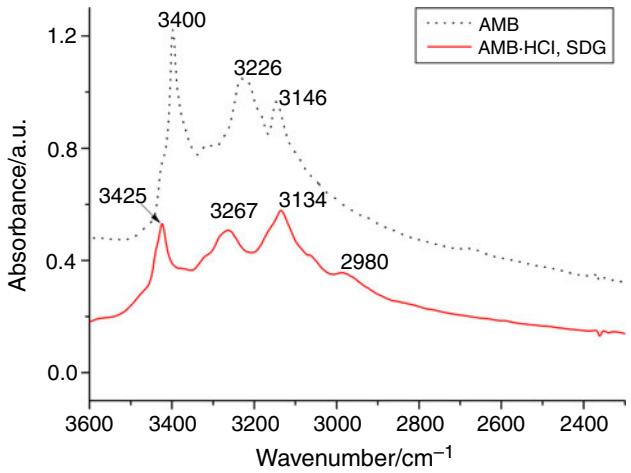

Fig. 3 FTIR spectra of AMB and AMB·HCl, 3600–2300 cm^{-1} spectral region

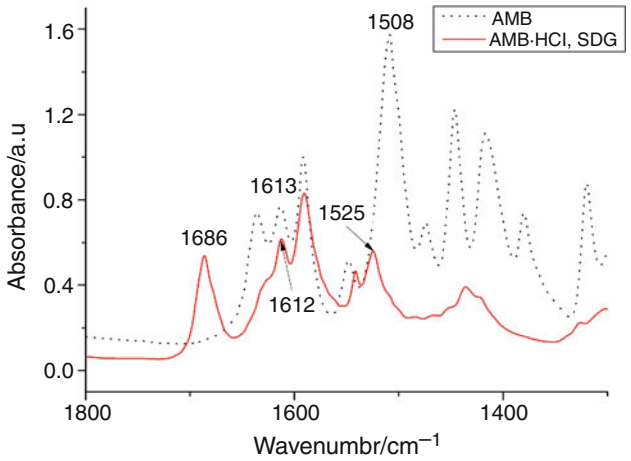

Fig. 4 FTIR spectra of AMB and AMB·HCl, 1800–1300 cm^{-1} spectral region

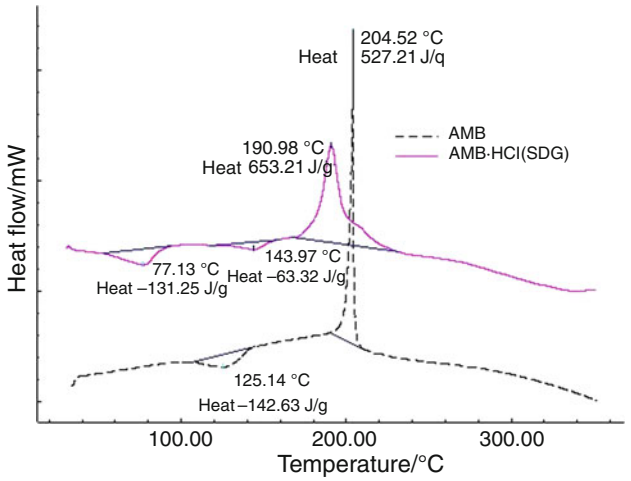

Fig. 5 DSC of AMB and AMB·HCl obtained by SDG

contains the secondary amine vibration at 1508 cm^{-1} which is shifted to 1525 cm^{-1} for the ambazone HCl spectrum.

In the spectrum of the salt a new strong absorption appeared at ~1686 cm^{-1}, which is assigned to deformation vibration of the protonated secondary amino group [26] (Fig. 4).

This frequency is not present in the FTIR spectrum of pure AMB, i.e., a hydrochloride was formed.

Thermal analysis DSC–DTA–TG

The DSC curves of the pure AMB and of the compound obtained by solvent-drop grinding (SDG) between AMB and HCl are presented in Fig. 5. The curve for the pure AMB revealed a broad endothermic signal from 105 to 143 °C, with a maximum at 125 °C and $\Delta H = 36$ kJ/mol, that corresponds to the loss of the water followed by a

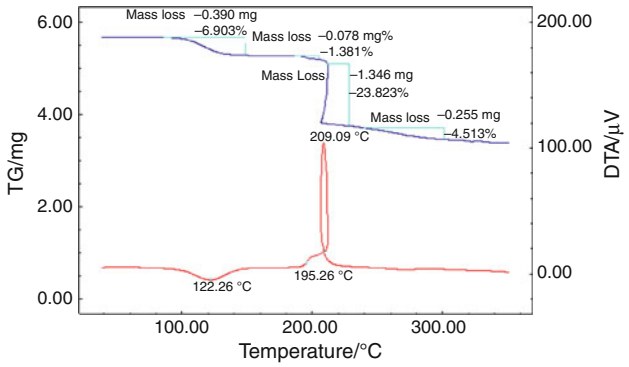

Fig. 6 DTA–TG of AMB

sharp exothermic signal at 204 °C, $\Delta H = 75$ kJ/mol due to the melting with decomposition of AMB.

The DSC curve of AMB·HCl presents three signals: a broad endothermic peak between 55 and 95 °C, with $\Delta H = 38$ kJ/mol, corresponding to the loss of non-bonding water molecules, an other broad endothermic peak between 121 and 160 °C, $\Delta H = 18$ kJ/mol due probably to the loss of HCl and an exothermic peak at 190 °C with $\Delta H = 185$ kJ/mol corresponding to the melting with decomposition of the sample.

The simultaneously DTA–TG measurements of the AMB reveal the thermal behavior of this compound (Fig. 6). TG–DTA traces of AMB show thermal stability until 90 °C. Between 86 and 149 °C the first mass loss occurs, with loss of 6.9%, corresponding to a broad endotherm peak between 100 and 140 °C with maximum at 122 °C due to water loss. Next mass losses occur in four steps: 1.168% in the range 187–200 °C, 1.8% in the range 203–211 °C, 23.88% in the range 211–228 °C corresponding to an exotherm on the DTA curve between 190 and 220 °C with peak maximum at 209 °C. These signals correspond to the mass loss by decomposition of the AMB. In the 239–301 °C range the decomposition continued with the 4.5% final mass loss, probably the elimination of the volatile components. The obtained data present a very good similarity with DSC measurements.

The DTA–TG measurements of the AMB·HCl reveal the thermal behavior of the compound obtained by SDG method (Fig. 7). TG–DTA traces of AMB·HCl indicate in the 90–135 °C temperature range the first mass loss of 5.34%, corresponding to a broad endotherm peak between 90 and 147 °C with maximum at 127 °C due to the water elimination. The second mass loss between 176 and 210 °C with loss of 9%, probably due to HCl elimination in the range of 250–350 °C, produces the final mass loss of 23.88%. Both steps of mass losses correspond to a sharp exotherm with T_{onset} at 172 °C and peak maximum at 190 °C. These signals have good similarity with DSC measurements.

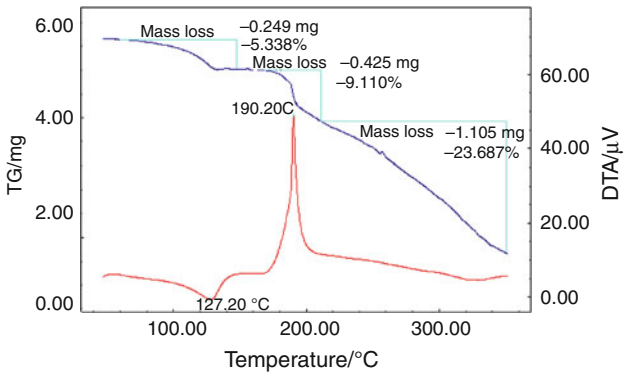

Fig. 7 DTA–TG of AMB·HCl obtained by SDG

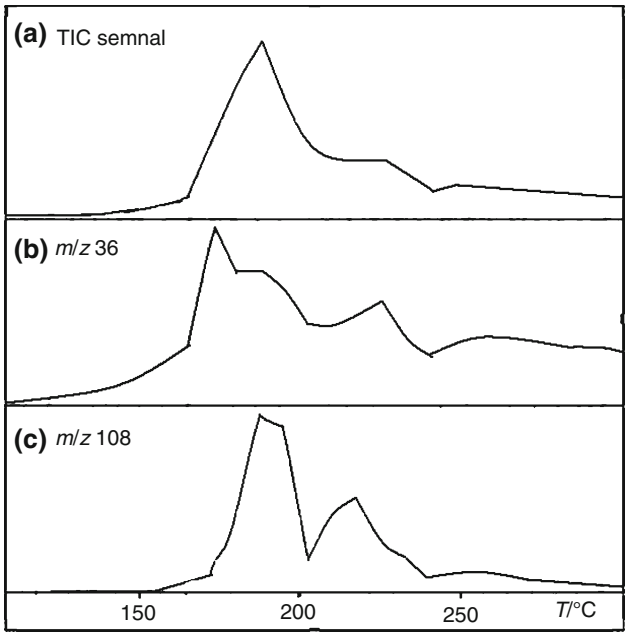

Fig. 8 The mass spectrometric signal: **a** TIC, **b** *m/z* 36 (HCl), and **c** *m/z* 108 (AMB) registered in experiment of thermal experiment in the range of 25–350 °C for AMB·HCl

Mass spectrometer

The mass spectrometer with a heated direct introduction system offers a rapid and precise instrument to perform pharmaceutical analysis [27]. The AMB and AMB·HCl was heated in the 25–350 °C temperature range with a slope of about 25 °C/min. In all this time mass spectra (one mass spectrum at 5 s) were registered. The quantity of compounds was measured by characteristic ions (see Fig. 8: *m/z* main 108 for ambazone and *m/z* 36 for Hydrochloric acid).

The important points observed are shown in Table 1.

The study of mass spectra at different temperatures shows the following:

Table 1 The starting and top temperature (°C) for hydrochloric acid and AMB in the 25–350 °C temperature range heating experiment

AMB/HCl ratio	HCl		AMB	
	Starting point	Top point	Starting point	Top point
1/1.08	125	180	160	195

The released quantity was monitored by characteristic ions (*m/z* 36 for HCl, and 108 for AMB, respectively)

- In every mass spectrum only the characteristic peaks of AMB and HCl can be seen;
- There were no observed peaks produced by new compounds;
- The top of maximum quantity for HCl and AMB was close but the starting point of HCl is significant before (35 °C).

All these observations lead to the conclusion that we have an ambazone hydrochloride salt.

^{13}C and ^{15}N NMR spectroscopy

The ^{13}C CP/MAS spectra of the AMB and AMB·HCl are shown in Fig. 9, where the asterisks indicate spinning sidebands. Both spectra consist of eight resonance lines, corresponding to the eight carbon sites in the molecular structure of the studied compounds. The main feature of these ^{13}C CP/MAS spectra is the important shift of the resonance lines of AMB·HCl compound compared with the similar spectrum which correspond to pure AMB. Most probably this line shift can be attributed to the aromatic ring current effect, which is relevant to NMR spectroscopy, as it dramatically influence the chemical shifts of ^{13}C and ^{1}H in organic molecules which contain benzene rings [28]. The magnitude of the ring current effect is less intense in the AMB·HCl compound, which could indicate that the Cl^- disrupts a possible π–π stacking in AMB. Another important result which can be obtained from ^{13}C CP/MAS spectra is about the number of independent molecules in the asymmetric unit. For asymmetric units containing more than one molecule, all the resonance lines for a given nucleus will be generally multiplied by the number of such molecules. Since all the AMB and AMB·HCl resonance lines are not multiplied, we can draw the conclusion that there is only one molecule per asymmetric unit of both investigated compounds.

The ^{15}N CP/MAS spectrum consists of seven resonance lines, according to the molecular structure of AMB·HCl. These lines are assigned as follows: two $–NH_2$ groups with resonances at 44.3 and 45.8 ppm; a $–NH_2^+$ group with the resonance line at 105.6 ppm; two –NH– groups at 141 and 171.5 ppm, respectively, and two non-protonated nitrogens

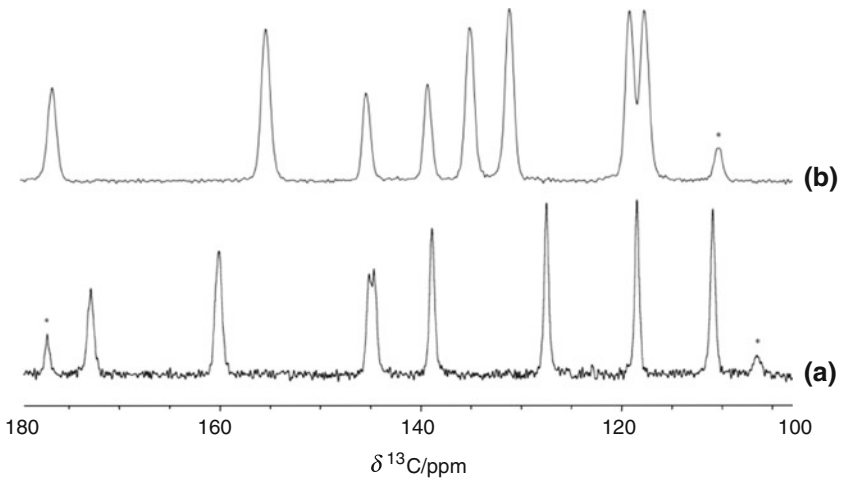

Fig. 9 The ^{13}C CP/MAS NMR spectra of **a** AMB and **b** AMB·HCl, recorded at a spinning frequency $\nu_R = 10$ kHz with a CP contact pulse of 1.5 ms. The asterisks indicate spinning sidebands

linked to the aromatic ring, which exhibit resonances at 266 and 282.8 ppm.

X-ray photoelectron spectroscopy

Both samples, AMB and AMB·HCl, were also analyzed by XPS technique in order to evaluate the atomic composition and chemical environment of the outermost 2–10 nm of the surface. Survey and core level spectra of the main elements (C 1s, N 1s, O 1s, S 1s) were recorded for the respective samples.

The XPS survey spectra of AMB and AMB·HCl are presented in Fig. 10 and the elemental composition determined from survey spectra are summarized in Table 2. The spectrum of ambazone consists mainly of features associated with carbon (C 1s), nitrogen (N 1s), sulphur (S 2p), and oxygen (O 1s) photoelectrons and corresponding Auger electron peaks. The elemental surface composition has been changed for AMB·HCl comparing with AMB. An additional peak feature is observed for chlorine (Cl 2p) once the HCl molecule was used to obtain the new solid form, and the measured C/N ratio shows a very slight difference (Table 2) between the two compounds.

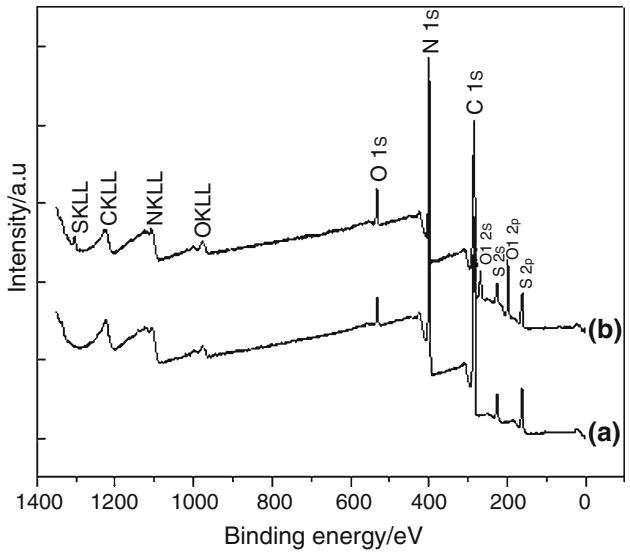

Fig. 10 XPS survey spectra recorded for the AMB (**a**) and AMB·HCl (**b**)

Table 2 Relative percentage of the main components for ambazone and AMB·HCl

Sample	Elemental composition/%					
	C	N	C/N	S	O	Cl
AMB	58.05	31.93	1.82	6.84	3.17	–
AMB·HCl	54.18	29.22	1.85	6.04	3.88	6.66

The detected O 1s signal is related to water molecules from monohydrate ambazone and hydroxyl groups presented to the samples surface adsorbed from environmental due to chemisorbed water molecules moisture.

XPS study shows that the N 1s core-level spectrum of the AMB base consists of a peak with a line width (FWHM) on the order of 3.1 eV. Upon protonation with HCl, the line width is slightly increased to 3.3 eV. The N 1s photopeaks were also curve-fitted as illustrated in Fig. 11. Photoemissions from the 1s core level nitrogen environments of AMB present two components, with the peak at 397 eV arising from simple nitrogen bonds and that at 399.4 eV from the C=N.

The N 1s photopeak for AMB·HCl presents an asymmetric shape and a high-binding energy line can be observed at 400.5 eV, due to the protonation of the secondary amine C=NH ($C=NH_2^+$) [29].

The results obtained by XPS study confirm the protonation of secondary amino groups as a proof of ambazone hydrochloride formation.

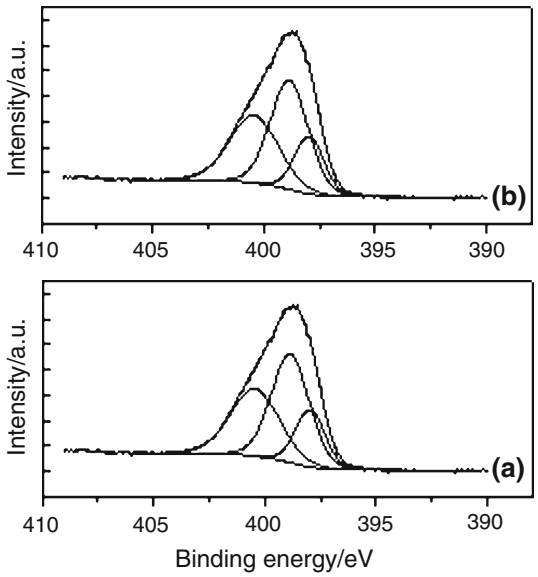

Fig. 11 N 1s high-resolution XPS spectra recorded for the AMB (**a**) and AMB·HCl (**b**)

Conclusions

Based on X-ray powder diffraction the lattice parameters and the space group for the new compound were determined.

FTIR and XPS data indicate the AMB·HCl formation by the appearance of the frequencies characteristic to NH_2^+ group.

DTA–TG–DSC curves for the salt obtained (AMB·HCl) are different as compared with those of pure AMB.

MS measurements confirm obtaining AMB·HCl, in an agreement with ^{13}C and ^{15}N NMR data which establishes that asymmetric unit contains one molecule.

Acknowledgements *Investing in people! PhD scholarship*, Project co-financed by the Sectoral Operational Programme Human Resources Development 2007–2013 Priority Axis 1 "Education and training in support for growth and development of a knowledge based society" Key area of intervention 1.5: Doctoral and post-doctoral programmes in support of research. Project POSDRU 6/1.5/S/3—"Doctoral Studies: Through Science Towards Society" Babeş-Bolyai University, Cluj-Napoca, Romania. The investigations were supported by the PN-II No. 61-003/2007 project.

References

1. Fulga I. Ambazone: Accepted notions, informations and possible perspectives. Pharmakon. 2006;56. www.pharmakon.ro/inc/arhiva/2006_02/Ambazona.pdf.
2. Lober G, Geller K, Hanschmann H, Popa LM, Repanovici R, Iliescu R, Romer W, Janke B, Kleinwachter V. Cationic anticancer drugs and their modes of action. Physiologie. 1989;26(4):305–16.
3. Fichtner I, Arnold W. Antineoplastic effect of 1,4-benzoquinone guanylhydrazone thiosemicarbazone in experimental tumor models. Pharmazie. 1983;38(2):130–1.
4. Kuhnel HJ, Amlacher R, Baumgart J, Schulze W. Distribution of 14C-ambazone in normal and leukemia P388-bearing mice. Arch Geschwulstforsch. 1988;58(4):217–22.
5. Kuhnel HJ, Amlacher R, Kramarczyk K, Schulze W. Pharmacokinetics of 14C-ambazone in rats. Pharmazie. 1988;43(3):197–9.
6. Baumgart J, Zhukovskaya NV, Anisimov VN. Carcinogenesis and aging. VIII. Effect of host age on tumour growth, metastatic potential and chemotherapeutic sensitivity to 1.4-benzoquinone-guanyl hydrazonethiosemicarbazone (ambazone) and 5-fluorouracil in mice and rats. Exp Pathol. 1988;33(4):239–48.
7. Amlacher R, Baumgart J, Hartl A, Weber H, Kuhnel HJ, Schulze W, Hoffmann H. Influence of age on antileukemic action, subacute toxicity and tissue distribution of ambazone in B6D2F1 mice. Arch Geschwulstforsch. 1990;60(1):11–8.
8. Amlacher R, Mackowiak A, Baumgart J, Schulze W, Hoffmann H. Influence of murine melanoma B16 on the distribution of ambazone in B6D2F1 mice. Pharmazie. 1990;45(5):379–80.
9. Gutsche W, Hartl A, Baumgart J, Schulze W. Antineoplastic activity and toxicity of dihydroambazone in comparison with ambazone (1,4-benzoquinone-guanylhydrazonethiosemicarbazone). Pharmazie. 1990;45(1):55–7.
10. Doring M. Mutagenic activity of ambazone in bacterial test systems. Stud Biophys. 1987;117(1–3):99–104.
11. http://www.pharmaceutical-int.com/categories/cocrystals/co-crystals-an-attractive-alternative-for-solid-forms.asp. Co-crystals—an attractive alternative for solid forms. 2007.
12. Brittain HG. Polymorphism in pharmaceutical solids. Drugs and the pharmaceutical sciences. 2nd ed., vol. 192. New York: Informa Healthcare; 2009.
13. Ling AR, Baker JL. Halogen derivatives of quinone. Part III. Derivatives of quinhydrone. J Chem Soc. 1893;63:1314–27.
14. Etter MC, Adsmond DA. The use of cocrystallization as a method of studying hydrogen bond preferences of 2-aminopyrimidine. J Chem Soc Chem Commun. 1990;589–91.
15. Etter MC, Reutzel SM, Choo CG. Self-organization of adenine and thymine in the solid state. J Am Chem Soc. 1993;115:4411–2.
16. Otsuka M, Otsuka K, Kaneniwa N. Relation between polymorphic transformation pathway during grinding and the physicochemical properties of bulk powders for pharmaceutical preparations. Drug Dev Ind Pharm. 1994;20:1649–60.
17. Pirttimaki J, Laine E, Ketolainen J, Paronen P. Effects of grinding and compression on crystal structure of anhydrous caffeine. Int J Pharm. 1993;95:93–9.
18. Shan N, Toda F, Jones W. Mechanochemistry and co-crystal formation: effect of solvent on reaction kinetics. Chem Commun (Camb.). 2002;20:2372–3.
19. Trask AV, Motherwell WDS, Jones W. Solvent-drop grinding: green polymorph control of crystallization. Chem Commun (Camb.). 2004;7:890–1.
20. Boultif A, Louër D. Powder pattern indexing with the successive dichotomy method. J Appl Cryst. 2004;37:724–31.
21. Ivanova B, Spiteller M. Salts of aromatic amines: crystal structures, spectroscopic and non-linear optical properties. Spectrochimica Acta A. doi:10.1016/j.saa.2010.08.017.
22. Koleva BB, Kolev T, Seidel RW, Spiteller M, Mayer-Figge H, Sheldrick WS. Self-assembly of hydrogensquarates: crystal structures and properties. J Phys Chem A. 2009;113(13):3088–95.
23. Heacock RA, Marion L. The infrared spectra of secondary amines and their salts. Can J Chem. 1956;34:1782–95.
24. Socrates G. Infrared and Raman characteristic group frequencies: tables and charts. 3rd ed. West Sussex: Wiley; 2001. p. 332.
25. Heacock RA, Marion L. The infrared spectra of secondary amines and their salts. Can J Chem. 1956;34(12):1782–95.

26. Cleaves AP, Plyler EK. The infra-red absorption spectrum of methylamine vapor. J Chem Phys. 1939;7:563–9.
27. Chernetsova ES, Bochkov PO, Ovcharov MV, Zhokhov SS, Abramovich RA. DART mass spectrometry: a fast screening of solid pharmaceuticals for the presence of an active ingredient, as an alternative for IR spectroscopy. Drug Test Anal. 2010;2: 292–4.
28. Gomes JANF, Mallion RB. Aromaticity and ring currents. Chem Rev. 2001;101(5):1349–84.
29. Stevens JS, Byard SJ, Muryn CA, Schroeder SLM, Identification of protonation state by XPS, solid-state NMR, and DFT: characterization of the nature of a new theophylline complex by experimental and computational methods. J Phys Chem B. doi: 10.1021/jp106465u.